

SIMULATION OF TEM DISLOCATION CONTRASTS

JOËL DOUIN
Laboratoire d'Etude des Microstructures
CNRS / ONERA, BP 72
92322 Châtillon Cedex
France

1. Introduction

A better understanding of the mechanisms governing the plastic properties of materials requires the analysis of the dislocations fine structure.

Important informations can be obtain using experimental methods at a macroscopic scale. For example, studying the slip traces at the surface of a deformed sample can help identifying the major slip systems activated during the deformation. However, in many cases, dislocations properties are directly related to local events occuring on their lines, as dissociation modes or interactions with points defects or precipitates. Direct observation of dislocations are thus necessary, and are achieved by using Transmission Electron Microscopy (TEM).

At a microscopic scale, High Resolution Electron Microscopy (HREM) may give precise informations by direct visualization of the distortion of the crystal in the close vicinity of the dislocation. However, HREM is not applicable at a mesoscopic scale since the dislocation under study must be straight and edge on in a very thin foil to be observed. Furthermore, no informations on the components of the displacements along the electron beam direction can be obtained from HREM images. On the contrary, imaging with conventional microscopy reveals information on the global geometry of the dislocations and on their interactions with other defects. Moreover, the resolution provided by weak-beam TEM allows for direct identification of dislocations as well as observation of dissociated dislocations.

The contrast of a dislocation image is a function of several parameters. Some are intrinsic to the material (anisotropic elasticity, absorption,...), some are extrinsic (imaging conditions, microscope, transfert function of the negative,...). The intrinsic parameters directly act on the diffracted amplitude or on the phase of the different beams.

Since the image of a dislocation is the result of the complex propagation of electrons through an anisotropic faulted crystal, the prediction of the image is a priori impossible, and precise interpretations of dislocations images require simulations.

In this course, we will first emphasize the dynamical interaction between the electron beams and the crystal (§ 2.3). We will then focus on approximations which are used in order to reduce the complexity of the calculations (§ 2.4). The description of the displacement field due to a dislocation is of prime importance and a way to calculate it in an anisotropic crystal will be described (§ 2.5). Finally, § 3. will be devoted to some real life examples.

2. Theory

2.1 ORIGIN OF CONTRAST

In the microscope, the almost parallel beam of electrons formed by the electron gun is scattered by the specimen. In the case of crystalline materials, this scattering takes the form of several diffracted beams (§ 2.2.2) travelling at small angles (≈ 1 or 2 degrees) with the incident beam.

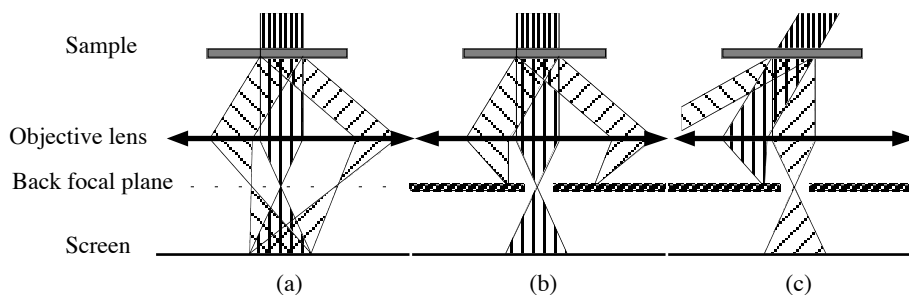


Figure 1 : Formation of an image within a Transmission Electron Microscope. (a) Scattering of the electron beam by a crystalline material ; (b) formation of a "bright field" image ; (c) formation of a "dark field" image. The diffraction angles have been exaggerated for the drawing.

These beams are focused by the objective lens to form a diffraction pattern in its back focal plane (Figure 1.a). The image is produced by selecting one or several beams by inserting an aperture in the focal plane of the objective lens. The contrast arises from local variation in the intensities of electrons scattered into Bragg's reflections from various parts of the thin specimen. When the aperture is inserted exactly on the objective lens axis, it does not allow diffraction beams to pass through to the final image, which is therefore formed by the direct beam and any low angle inelastic scattering (Figure 1.b). This type of image is called bright-field image. Images can also be formed by any one of the diffracted beam by either displacing the aperture to receive this beam, or by tilting the illumination so that the required beam passes down the axis of the objective (Figure 1.c). The resulting image is called a dark-field image.

2.2. DIFFRACTION OF ELECTRONS IN A PERFECT CRYSTAL

The exact description of the interaction of an electron beam with a crystal requires the use of quantum mechanic formulation and will be reported in § 2.3. In what follows, we will concentrate on an approximated way to describe this interaction in order to obtain a simple way to understand what is happening in the crystal and what are the characteristic of the beams going out of the crystal.

2.2.1 Kinematical Diffraction of Electrons in a Perfect Crystal

As a first approximation, we assume that the electrons of the incident beam are travelling in the same direction. We call λ the wave length of the electron beam in

vacuum oriented along the wave vector \mathbf{k} , such that $\|\mathbf{k}\| = 1/\lambda$. The amplitude of the incident beam A_0 is :

$$A_0 = 1/\|\mathbf{r}\| \exp(2i\pi \mathbf{k} \cdot \mathbf{r}) \quad (1)$$

where \mathbf{r} is a point of the wave front. The amplitude of the beam scattered by one atom, say number 1, is

$$A_1 = f_1(\theta)A_0 \quad (2)$$

where $f_1(\theta)$ is the scattering factor for this atom. The amplitude of the beam scattered by atom j is

$$f_j(\theta)A_0 \exp(i\varphi_j) \quad (3)$$

where φ_j , the phase shift between beams scattered by atom 1 and atom j , is :

$$\varphi_j = \frac{2\pi \delta}{\lambda} \quad (4)$$

and here the path difference $\delta = \lambda (\mathbf{k} - \mathbf{k}') \cdot \mathbf{r}_i$ (Figure 2), where \mathbf{r}_i describes the position of the atom i in the unit cell.

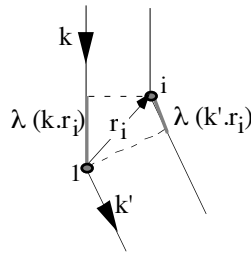


Figure 2

The scattered amplitude in the direction \mathbf{k}' resulting from the interaction of an electron beam \mathbf{k} and a unit cell is thus given by :

$$\phi = \frac{\exp(2i\pi \mathbf{k} \cdot \mathbf{r})}{r} \sum_i f_i(\theta) \exp(-2i\pi (\mathbf{k}' - \mathbf{k}) \cdot \mathbf{r}_i) \quad (5)$$

We can write the factor structure $F(\theta)$ of the unit cell as :

$$F(\theta) = \sum_i f_i(\theta) \exp(-2i\pi (\mathbf{k}' - \mathbf{k}) \cdot \mathbf{r}_i) \quad (6)$$

the summation being made over the atoms of the unit cell.

In the same way and leaving out the factor $\exp(2i\pi \mathbf{k} \cdot \mathbf{r})/r$ which is the propagation term, the scattered amplitude resulting from an assembly of unit cells is given by :

$$\phi = \sum_{\mathbf{n}} F(\theta) \exp\left(-2i\pi (\mathbf{k}' - \mathbf{k}) \cdot \mathbf{r}_{\mathbf{n}}\right) \quad (7)$$

Now the summation is made over all the unit cells and $\mathbf{r}_{\mathbf{n}}$ is defined by :

$$\mathbf{r}_{\mathbf{n}} = n_1 \mathbf{a} + n_2 \mathbf{b} + n_3 \mathbf{c} \quad (8)$$

where \mathbf{a} , \mathbf{b} and \mathbf{c} are the unit cell translations in the crystal, and n_1 , n_2 and n_3 are integers.

2.2.2 Conditions for Strong Diffraction in a Crystal

In terms of reciprocal lattice coordinates, $\mathbf{k} - \mathbf{k}'$ can be written as :

$$\mathbf{k}' - \mathbf{k} = \xi_1 \mathbf{a}^* + \xi_2 \mathbf{b}^* + \xi_3 \mathbf{c}^* \quad (9)$$

And ϕ then writes :

$$\phi = \sum_{\mathbf{n}} F(\theta) \exp\left(-2i\pi (n_1 \xi_1 + n_2 \xi_2 + n_3 \xi_3)\right) \quad (10)$$

Strong diffraction occurs when $(n_1 \xi_1 + n_2 \xi_2 + n_3 \xi_3)$ is an integer for all n_1 , n_2 and n_3 , that is when $\mathbf{k} - \mathbf{k}'$ coincides with a reciprocal lattice vector :

$$\mathbf{k}' - \mathbf{k} = \mathbf{g} = h \mathbf{a}^* + k \mathbf{b}^* + l \mathbf{c}^* \quad (11)$$

Note that since $\|\mathbf{g}\| = 1/d_{hkl}$ and $\|\mathbf{k} - \mathbf{k}'\| = 2 \sin(\theta_B)/\lambda$ (Figure 3), expression (9) is equivalent to the Bragg law :

$$\lambda = 2 d_{hkl} \sin(\theta_B) \quad (12)$$

which simply states that the (hkl) plane is in Bragg position.

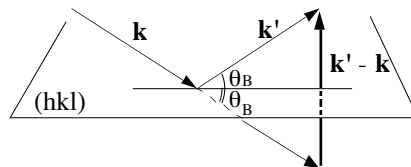


Figure 3

We can then derive a simple geometrical construction for determining the conditions of reflection : from the origin of the sample, we construct a sphere with radius $1/\lambda$, called the Ewald sphere (Figure 4). From the intersection of the Ewald sphere with the transmitted beam, we construct the reciprocal lattice of the crystal. Each point of the reciprocal lattice which intersects the Ewald sphere satisfies the Bragg conditions, and a strong Bragg reflection will occur if the diffracted beam is at the intersection of the reciprocal crystal with the Ewald sphere.

In TEM, the crystal is usually in the form of a plate and the intensity distribution in the reciprocal lattice as the form of a spike. Thus, reflection takes place not only for an exact Bragg reflections, but also over a range of orientations of the crystal corresponding to the intersections of the Ewald sphere with the spikes in the reciprocal lattice (Figure 4). In any case, the diffracted beam can be written as a function of the incident beam \mathbf{k} :

$$\mathbf{k}' = \mathbf{k} + \mathbf{g} + \mathbf{s}_g \quad (13)$$

where \mathbf{g} is a vector of the reciprocal lattice and \mathbf{s}_g is called the deviation from Bragg angle. \mathbf{s}_g is zero for an exact Bragg reflection.

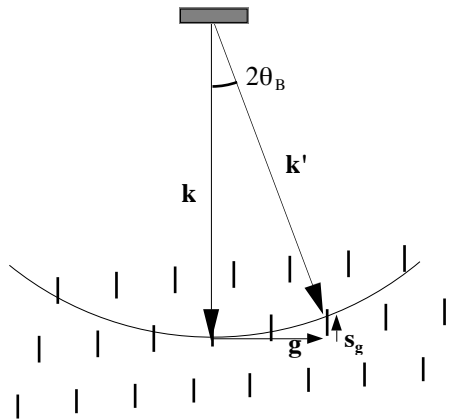


Figure 4 : Ewald construction

2.3. ELECTRON PROPAGATION IN A DEFORMED CRYSTAL

In what follows, we will use the wave-mechanical formalism. A complete treatment of the electron diffraction in imperfect crystals is not within the scope of this paper. The theory of electron diffraction summarized here is based on the dynamical theory formulated by Howie and Whelan [1] and Takagi [2] and described in great details by Hirsch et al. [3].

The Schrödinger's equation which describes the propagation of an electron subjected to a potential difference (or acceleration tension) E through a deformed crystal is :

$$\nabla^2 \psi(\mathbf{r}) + \frac{8\pi^2 m e}{h^2} (E + V'(\mathbf{r})) \psi(\mathbf{r}) = 0 \quad (14)$$

where $V'(\mathbf{r})$ is the potential of the deformed crystal, differing from the potential of the undefected crystal $V(\mathbf{r})$ by a small perturbation. Equation (14) has no general solution, but in order to solve it, we will consider that the potential $V'(\mathbf{r})$, as $V(\mathbf{r})$, varies smoothly within the unit cell. Since the atom at the position \mathbf{r}_a in the perfect crystal is moved by the quantity $\mathbf{R}(\mathbf{r}_a)$, where $\mathbf{R}(\mathbf{r})$ represents the deformation of the crystal at point \mathbf{r} , $V'(\mathbf{r}_a) = V(\mathbf{r}_a - \mathbf{R}(\mathbf{r}_a))$. $V'(\mathbf{r})$ is small in regards to E (typically in the order of 10

to 20 V compared with an acceleration tension often larger than 100 kV) and again provided that the crystal potential deforms smoothly, it can then be written as a Fourier serie over the reciprocal vectors \mathbf{g} :

$$V(\mathbf{r}) = \left(\frac{\hbar^2}{2me} \right) \sum_{\mathbf{g}} \left(u_{\mathbf{g}}(\mathbf{r}) \exp(-2i\pi \mathbf{g} \cdot (\mathbf{r} - \mathbf{R}(\mathbf{r}))) \right) \quad (15)$$

A solution for the above Schrödinger's equation has the form :

$$\psi(\mathbf{r}) = \sum_{\mathbf{g}} \phi_{\mathbf{g}}(\mathbf{r}) \exp(2i\pi \mathbf{k}' \cdot \mathbf{r}) \quad (16)$$

where the magnitude of \mathbf{k}' , the wave vector of the diffracted beam, is given by the conservation of energy :

$$\frac{\hbar^2 \|\mathbf{k}'\|^2}{2m} = eE \quad (17)$$

Substituting (15) and (16) in equation (14), we obtain :

$$\sum_{\mathbf{g}} \left\{ \frac{1}{4\pi^2} \nabla^2 \phi_{\mathbf{g}}(\mathbf{r}) + \frac{i}{\pi} (\mathbf{k} + \mathbf{g} + \mathbf{s}_{\mathbf{g}}) \cdot \nabla \phi_{\mathbf{g}}(\mathbf{r}) + \sum_{\mathbf{h}} u_{\mathbf{g}-\mathbf{h}}(\mathbf{r}) \phi_{\mathbf{h}}(\mathbf{r}) \exp\left(2i\pi(\mathbf{h}-\mathbf{g}) \cdot \mathbf{R}(\mathbf{r}) + 2i\pi(\mathbf{s}_{\mathbf{h}}-\mathbf{s}_{\mathbf{g}}) \cdot \mathbf{r}\right) \right\} \exp(2i\pi (\mathbf{k} + \mathbf{g} + \mathbf{s}_{\mathbf{g}}) \cdot \mathbf{r}) = 0 \quad (18)$$

where the scattered wave vector has been expressed using expression 13. In order for the equations (18) to be satisfied, the terms in the large brackets must be zero. Provided that $\mathbf{R}(\mathbf{r})$ varies slowly with \mathbf{r} and that $\nabla^2 \phi_{\mathbf{g}}(\mathbf{r})$ is negligible in comparison with $(\mathbf{k} + \mathbf{g} + \mathbf{s}_{\mathbf{g}}) \cdot \nabla \phi_{\mathbf{g}}(\mathbf{r})$, equations (18) reduce then to :

$$\frac{\partial \phi_{\mathbf{g}}(\mathbf{r})}{\partial \eta_{\mathbf{g}}} = \frac{i\pi}{\|\mathbf{k} + \mathbf{g} + \mathbf{s}_{\mathbf{g}}\|} \sum_{\mathbf{h}} u_{\mathbf{g}-\mathbf{h}}(\mathbf{r}) \phi_{\mathbf{h}}(\mathbf{r}) \exp\left(2i\pi(\mathbf{h}-\mathbf{g}) \cdot \mathbf{R}(\mathbf{r}) + 2i\pi(\mathbf{s}_{\mathbf{h}}-\mathbf{s}_{\mathbf{g}}) \cdot \mathbf{r}\right) \quad (19)$$

where $\eta_{\mathbf{g}}$ is the co-ordinate in the direction of the diffracted beam \mathbf{k}' .

Equations (19) can be rewritten using the wave-optical formulation by introducing the extinction distance $\xi_{\mathbf{g}}$. By definition, $\xi_{\mathbf{g}}$ is twice the distance in the crystal that a diffracted beam \mathbf{g} has to cross in order to build up to unit amplitude. If $V_{\mathbf{c}}$ is the volume of the unit cell and $F_{\mathbf{g}}$ its structure factor (expression 6), it can be shown that :

$$\xi_{\mathbf{g}} = \frac{\pi V_{\mathbf{c}} \cos \theta_{\mathbf{g}}}{\lambda F_{\mathbf{g}}} \quad (20)$$

Alternatively, $\xi_{\mathbf{g}}$ writes :

$$\xi_{\mathbf{g}} = \frac{\|\mathbf{k}'\| \cos \theta_{\mathbf{g}}}{u_{\mathbf{g}}(\mathbf{r})} \approx \frac{\|\mathbf{k}\|}{u_{\mathbf{g}}(\mathbf{r})} \quad (21)$$

since, for electrons in the crystal, Bragg angles θ_B are small (of the order of 10^{-2} rad). It follows that :

$$\frac{u_{\mathbf{g}-\mathbf{h}}(\mathbf{r})}{\|\mathbf{k}+\mathbf{g}+\mathbf{s}_{\mathbf{g}}\|} \approx \frac{1}{\xi_{\mathbf{g}-\mathbf{h}}} \quad (22)$$

and equations (18) transform into the equivalent form :

$$\frac{\partial \phi_{\mathbf{g}}(\mathbf{r})}{\partial \eta_{\mathbf{g}}} = \sum_{\mathbf{h}} \frac{i\pi}{\xi_{\mathbf{g}-\mathbf{h}}} \phi_{\mathbf{h}}(\mathbf{r}) \exp\left(2i\pi(\mathbf{h}-\mathbf{g}) \cdot \mathbf{R}(\mathbf{r}) + 2i\pi(\mathbf{s}_{\mathbf{h}}-\mathbf{s}_{\mathbf{g}}) \cdot \mathbf{r}\right) \quad (23)$$

Of course, the observed intensity of the beam is : $I = \phi_{\mathbf{g}} \phi_{\mathbf{g}}^*$

Notice finally that, while electrons do not disappear in the crystal, some of them undergo large angle, eventually inelastic, scattering. This can be taken into account in equations (23) by replacing $1/\xi_{\mathbf{g}}$ by $1/\xi_{\mathbf{g}} + i/\xi_{\mathbf{g}}'$, where $\xi_{\mathbf{g}}'$ are phenomenological parameters and the ratios $\xi_{\mathbf{g}}/\xi_{\mathbf{g}}'$ are called anomalous absorption parameters.

2.4 APPLICATIONS OF THE DIFFRACTION THEORY TO ELECTRON MICROSCOPY

In order to calculate the scattered beams $\phi_{\mathbf{g}}$, equations (23) have to be integrated for every beams as a function of $\eta_{\mathbf{g}}$, that is along the directions $\mathbf{k} + \mathbf{g} + \mathbf{s}_{\mathbf{g}}$. This implies taking into account of derivative of $\phi_{\mathbf{g}}$ as a function of x, y and z. Such an integration is usually intractable by analytical techniques and requires to be numerically computed. However, the level of complexity is such that, for the time being, there is no program available containing no further approximations than the ones described above.

Two approximations are commonly used : (i) directions \mathbf{k} and \mathbf{k}' are nearly parallel, and integration is approximated along the diffracted beam \mathbf{k}' , that is along the z axis ; (ii) very often only two beams play a significant role in the formation of the image : the transmitted beam and a diffracted beam, and the effect of the other beams is neglected.

2.4.1 Column Approximation

At the bottom surface of the sample, the contribution of the electrons to the intensity on a point in the exit surface of the sample is coming at most from an area which is at the base of a cone (figure 5).

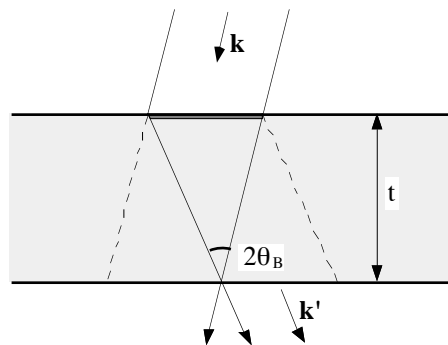


Figure 5

The size of the contributing area on the top surface of the sample is a function of θ_B and of the thickness t of the foil, and is approximately $2 t \theta_B$. At maximum, θ_B is in the order of 10^{-2} rad. The beams contributing to the image are thus coming from an area at most 2 nm in diameter for a foil thickness of 100 nm. It follows that, provided that \mathbf{R} does not vary rapidly, the terms in $\partial/\partial x$ and $\partial/\partial y$ in equations (23) may be ignored. In the column approximation, the beams are thus considered as parallel within a narrow cylinder parallel to the diffracted beam. In this approximation \mathbf{s}_g is parallel to the diffracted beam \mathbf{k}' and is referred as s or s_z , the positive being in the z direction. Notice that beams with Bragg angles larger than 2 degrees have extinction distances usually very large, which in regard to equation (23) indicate that they should contribute very little. However, equation (23) also show that not only beams with small extinction distances but beams with small deviation from Bragg angle contribute strongly to the image too. Thus, the column approximation will be suitable provided that no small beam other than \mathbf{g} is strongly excited.

2.4.2 Many-Beams Calculation in the Column Approximation

Within the framework of column approximation, equations (23) can be written in a matrix form :

$$\frac{d \Phi(\mathbf{r})}{dz} = \mathbf{M} \Phi(\mathbf{r}) \quad (24)$$

where $\Phi(\mathbf{r})$ is the vector

$$\Phi(\mathbf{r}) = \begin{bmatrix} \phi_0(\mathbf{r}) \\ \phi_1(\mathbf{r}) \\ \vdots \\ \phi_n(\mathbf{r}) \end{bmatrix} \quad (25)$$

Equations (24) describe the interaction of $(n+1)$ beams (transmitted beam is beam 0) contributing to the image. Using the wave-optical formulation, the symmetrical matrix \mathbf{M} writes :

$$\begin{bmatrix} M_{00} & M_{01} & \cdots & M_{0q} & \cdots & M_{0n} \\ M_{01} & M_{11} & & & & \\ \vdots & & \ddots & & & \\ M_{0q} & & & M_{qq} & & \\ \vdots & & & M_{pq} & \ddots & \\ M_{0n} & & & & & M_{nn} \end{bmatrix} \quad (26)$$

$$\text{when } p \neq q : M_{pq} = i \xi_1 \left(\frac{1}{\xi_{p-q}} + \frac{i}{\xi_{p-q}} \right), \text{ giving } M_{0q} = i \xi_1 \left(\frac{1}{\xi_q} + \frac{i}{\xi_q} \right)$$

$$\text{and } M_{qq} = \left[-\frac{\xi_1}{\xi_0} + 2is_q \xi_1 + 2i\pi \frac{d \mathbf{g}_q \cdot \mathbf{R}}{dz} \right] \text{ which reduces to } M_{00} = -\frac{\xi_1}{\xi_0} \text{ for } q = 0.$$

2.4.3 Two Beams Calculations

By forming an image of the back focal plane of the objective lens with the microscope, it is possible to directly determine which beams are excited since they will appear as strong spots in the diffraction pattern (§ 2.2). It is possible to tilt the sample in such a way that only one row of the reciprocal lattice parallel to beam \mathbf{g} is in or near Bragg conditions. Head et al. [4] have shown that more than 80% of the total intensity is contained within the transmitted beam and the diffracted beam \mathbf{g} . Assuming that these two beams only contribute significantly to the image, the equations (23) simplify to a set of two coupled differential equations :

$$\left\{ \begin{array}{l} \frac{\partial \Phi_0}{\partial z} - \frac{\partial \Phi_0}{\partial x_{\mathbf{g}}} \operatorname{tg} \theta_B = \frac{i\pi}{\xi_0} \Phi_0 + \frac{i\pi}{\xi_{\mathbf{g}}} \Phi_{\mathbf{g}} \exp(2i\pi(\mathbf{g}\mathbf{R} + \mathbf{s}_{\mathbf{g}}\mathbf{r})) \\ \frac{\partial \Phi_{\mathbf{g}}}{\partial z} + \frac{\partial \Phi_{\mathbf{g}}}{\partial x_{\mathbf{g}}} \operatorname{tg} \theta_B = \frac{i\pi}{\xi_0} \Phi_0 \exp(-2i\pi(\mathbf{g}\mathbf{R} + \mathbf{s}_{\mathbf{g}}\mathbf{r})) + \frac{i\pi}{\xi_{\mathbf{g}}} \Phi_{\mathbf{g}} \end{array} \right. \quad (27)$$

where z is the co-ordinate in the direction of the transmitted beam and $x_{\mathbf{g}}$ the component of $\eta_{\mathbf{g}}$ perpendicularly to the transmitted beam. In the wave-optical formulation, these equations can be written using the phenomenological complex values $\xi_{\mathbf{g}}$ and $\xi'_{\mathbf{g}}$:

$$\left\{ \begin{array}{l} \frac{\partial \Phi_0}{\partial z} - \frac{\partial \Phi_0}{\partial x_{\mathbf{g}}} \operatorname{tg} \theta_B = -\frac{\xi_{\mathbf{g}}}{\xi_0} \Phi_0 + \left(i - \frac{\xi_{\mathbf{g}}}{\xi_0} \right) \Phi_{\mathbf{g}} \\ \frac{\partial \Phi_{\mathbf{g}}}{\partial z} + \frac{\partial \Phi_{\mathbf{g}}}{\partial x_{\mathbf{g}}} \operatorname{tg} \theta_B = \left(i - \frac{\xi_{\mathbf{g}}}{\xi_0} \right) \Phi_0 + \left(\frac{\xi_{\mathbf{g}}}{\xi_0} + 2is\xi_{\mathbf{g}} - 2i\frac{\partial \mathbf{g}\mathbf{R}}{\partial z} - 2i\frac{\partial \mathbf{g}\mathbf{R}}{\partial x_{\mathbf{g}}} \operatorname{tg} \theta_B \right) \Phi_{\mathbf{g}} \end{array} \right. \quad (28)$$

It is worth emphasizing that these equations show that the contrast is in fact a function of the derivative of the product $\mathbf{g}\mathbf{R}$, rather than \mathbf{R} .

2.4.4 Two Beams in Column Approximation

When only two beams are taken into account within the column approximation, equations (28) simply reduce to

$$\left\{ \begin{array}{l} \frac{d\Phi_0}{dz} = -\frac{\xi_{\mathbf{g}}}{\xi_0} \Phi_0 + \left(i - \frac{\xi_{\mathbf{g}}}{\xi_0} \right) \Phi_{\mathbf{g}} \\ \frac{d\Phi_{\mathbf{g}}}{dz} = \left(i - \frac{\xi_{\mathbf{g}}}{\xi_0} \right) \Phi_0 + \left(\frac{\xi_{\mathbf{g}}}{\xi_0} + 2is\xi_{\mathbf{g}} - 2i\frac{\partial \mathbf{g}\mathbf{R}}{\partial z} \right) \Phi_{\mathbf{g}} \end{array} \right. \quad (29)$$

which are the equations used in programs "ONEDIS" and "TWOEDIS" by Head et al [4].

2.4.5 Kinematical Approximation

Finally, assuming that the two beams and column approximations are operative, the last step of simplification is to consider that the diffracted beam is weak compared to the transmitted beam, the latter being now taken as constant. In such a case, the amplitude of the diffracted beam can be written as :

$$\Phi_{\mathbf{g}} = \frac{i\pi}{\xi_{\mathbf{g}}} \int_0^t \exp(-2i\pi(\mathbf{g}\mathbf{R} + s\mathbf{z})) dz \quad (30)$$

where t is the thickness of the foil. This equation is often used in order to obtain a first and quick idea of what you should obtain (see § 3.1).

2.5 DISPLACEMENT FIELD AROUND A DISLOCATION

The fact that calculation of the image requires the displacement field due to a dislocation to be known precisely in a continuous way and over a large scale has been hidden above. This displacement field can be attained by different methods, from isotropic elasticity to atomistic simulations. However, atomistic simulations which often require long calculation time for a limited area under study, are for the time being inappropriate and in what follows, we will use linear elasticity.

Crystals are often anisotropic. Since anisotropy can modify the image of a dislocation in a very strong way (see § 3.1), anisotropic elasticity must be used in order to compare direct observations of dislocations and simulated images. Notice, however, that the exact displacement in a thin foil is intractable if account is taken of anisotropic elasticity and the effects of surfaces. The latter is not included in this paper. In what follows, we will use Stroh's formalism [5] with Head et al. notations [4].

2.5.1 Anisotropic Elasticity

The stresses σ_{ij} are related to the elastic displacements R_k by the equations :

$$\sigma_{ij} = \sum_{k,l} c_{ijkl} \frac{\partial R_k}{\partial x_l} \quad (31)$$

where i, j, k and l can take the values 1, 2 or 3. On substituting the values of σ in the equilibrium equations in the absence of external forces,

$$\vec{\Delta}\sigma = 0 \quad \text{or} \quad \sum_i \frac{\partial \sigma_{ij}}{\partial x_j} = 0 \quad (32)$$

we found :

$$\sum_{j,k,l} c_{ijkl} \frac{\partial^2 R_k}{\partial x_j \partial x_l} = 0 \quad (33)$$

For an infinite defect along the x_3 axis (Figure 6), solutions of the above equations, independent of x_3 , have the form :

$$R_k = A_k f(x_1 + p x_2) \quad (34)$$

provided that the constant vector A_k satisfies :

$$\sum_i \left(c_{i1k1} + p c_{i1k2} + p c_{i2k1} + p^2 c_{i2k2} \right) \cdot A_k = 0 \quad (35)$$

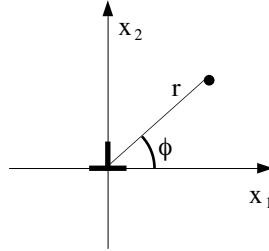


Figure 6 : Coordinate system used for the calculation of displacement field \mathbf{R} . The dislocation line is parallel to the x_3 -axis which points towards the figure. The angle ϕ is in the plane normal to the dislocation line and is measured from the slip plane.

Values not identically zero of the vector A_k can be found if the determinant associated to the set of equations (35) is zero, that is, if p is a root of the sextic equation :

$$\left| c_{i1k1} + p c_{i1k2} + p c_{i2k1} + p^2 c_{i2k2} \right| = 0 \quad (36)$$

From energy arguments, it can be shown that the roots of equation (36) occur in complex conjugate pairs p_α ($\alpha = 1, 2$ or 3), and a general expression of the displacements is :

$$R_k = \sum_{\alpha} A_{k\alpha} f_{\alpha}(x_1 + p_{\alpha} x_2) + \text{complex conjugate} \quad (37)$$

2.5.2 Case of a Dislocation

Consider now the displacements with the following form :

$$R_k = \frac{1}{2i\pi} \sum_{\alpha} A_{k\alpha} D_{\alpha} \text{Ln}(x_1 + p_{\alpha} x_2) + \text{c.c.} \quad (38)$$

where the D_{α} are constant. Along a closed path encircling x_3 , R_k changes by an amount :

$$b_k = \sum_{\alpha} A_{k\alpha} D_{\alpha} + \text{c.c.} \quad (39)$$

and the resultant force acting across a closed path encircling x_3 is :

$$F_i = \sum_{\alpha} L_{i\alpha} D_{\alpha} + c.c. \quad (40)$$

where the three vectors $L_{i\alpha}$ are defined by :

$$L_{i\alpha} = \sum_k \left(c_{i2k1} + p_{\alpha} c_{i2k2} \right) A_{k\alpha} \quad (41)$$

Equations (38) will then represent the displacements due to an infinite dislocation along x_3 , provided that b_k is the Burgers vector of the dislocation (equation 39), and provided that there is no net force along its axis, that is :

$$F_i = 0 \text{ or } \sum_{\alpha} \sum_k \left(c_{i2k1} + p_{\alpha} c_{i2k2} \right) A_{k\alpha} D_{\alpha} = 0 \quad (42)$$

It follows that the displacement field \mathbf{R} can be determined as follows :

- first find the roots p_{α} from equation (36), and thus the vectors \mathbf{A}_k
- then determine the three complex constants D_{α} from equations (39) and (42)

Notice that since expression (36) is a sextic equation, there is no general analytical form for its solutions. Equation (36) has to be solved numerically, except in some special cases, extensively described by Steeds [6]. Head et al. [4] have developed a procedure called ANCALC which automatically calculate the values \mathbf{A}_k , D_{α} et p_{α} .

3. Exemples of the Use of Simulations

3.1. INFLUENCE OF ANISOTROPIC ELASTICITY IN THE EXTINCTION CONDITIONS

In isotropic elasticity, the displacement $\mathbf{R} = (R_1, R_2, R_3)$ near a dislocation at a point (r, ϕ) (Figure 6) is :

$$\mathbf{R} = \frac{1}{2\pi} \left\{ \mathbf{b}\phi + \mathbf{b}_e \frac{\sin 2\phi}{4(1-\nu)} + \mathbf{b} \times \mathbf{u} \left(\frac{1-2\nu}{2(1-\nu)} \ln r + \frac{\cos 2\phi}{4(1-\nu)} \right) \right\} \quad (43)$$

where \mathbf{b}_e is the edge component of the Burgers vector \mathbf{b} , and \mathbf{u} its line. This simply reduces to

$$\mathbf{R} = \frac{\mathbf{b}\phi}{2\pi} \quad (44)$$

for a pure screw dislocation (\mathbf{b}/\mathbf{u}). Thus, in isotropic crystals and under the kinematical approximation (equation 30), a screw dislocation is out of contrast when $\mathbf{g}\cdot\mathbf{b} = 0$, since in that case, there is no difference between the beam diffracted by a perfect and a faulted crystal. This holds true for dislocations containing an edge character, provided that the quantity $\mathbf{g}\cdot(\mathbf{b}\times\mathbf{u})$ is small enough. The corresponding " $\mathbf{g}\cdot\mathbf{b} = 0$ invisibility criterion" provides a quick and simple way to determine the direction of \mathbf{b} that consists in searching two independent reflections under which the defect is invisible.

In anisotropic crystals observed under dynamical conditions, the $\mathbf{g}\cdot\mathbf{b} = 0$ invisibility criterion is however often unapplicable. This is exemplified in figure 7.a which shows that in β -CuZn, a screw dislocation with a Burgers vector $\mathbf{b} = [111]$, imaged with $\mathbf{g} = 1, 1, \bar{2}$, still exhibits a significant contrast in condition $\mathbf{g}\cdot\mathbf{b} = 0$. However, simulations show that imaging with an large deviation s_g from Bragg angle (the "weak beam" technique) extends the applicability of the $\mathbf{g}\cdot\mathbf{b} = 0$ invisibility criterion since, provided the Bragg deviation is large enough, the $\mathbf{g}\cdot\mathbf{b} = 0$ holds true (figures 7.b, c and d).

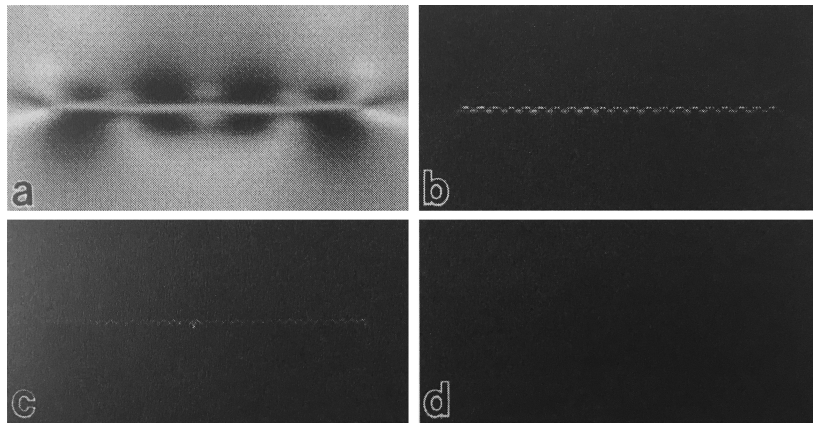


Figure 7 : Simulated images of a $[111]$ screw dislocation under $\mathbf{g}\cdot\mathbf{b} = 0$ condition. ($\mathbf{g} = 1, 1, \bar{2}$) (a) bright field image under Bragg condition ($s_g = 0$) ; (b) dark field (DF) image, $s_g = 0.2 \text{ nm}^{-1}$; (c) DF, $s_g = 0.3 \text{ nm}^{-1}$; (d) DF, $s_g = 0.4 \text{ nm}^{-1}$. The grey scale is identical for every dark field pictures (i.e. the exposure time is constant). The simulations have been performed using the "Cufour" program, a many-beams program with column approximation by Schäublin and Stadelmann [7].

3.2 ARTEFACT DUE TO MANY-BEAMS INTERACTION

Double contrast of superpartials with Burgers vector $1/2[110]$ has been repeatedly reported in condition $\mathbf{g}\cdot\mathbf{b} = 2$ in several intermetallics with $L1_2$ structure. This double contrast has been interpreted as a proof of dissociation of these dislocations, leading to different modelizations of slip glide processes. Numeric simulations of dislocation images have shown that the double contrast is an artefact arising for a small and well-defined Bragg deviation range (Figure 8). The doubling of the contrast occurs around the $\mathbf{g}\cdot\mathbf{b} = 2$ conditions (when the image is done with beam \mathbf{g} while beam $3\mathbf{g}$ is excited), and is absent when calculations are made using only two beams. This latter point indicates that the artefact is related to a double diffraction at the core of the dislocation resulting from an intensity transfer from beam \mathbf{g} or $-\mathbf{g}$ to $2\mathbf{g}$.

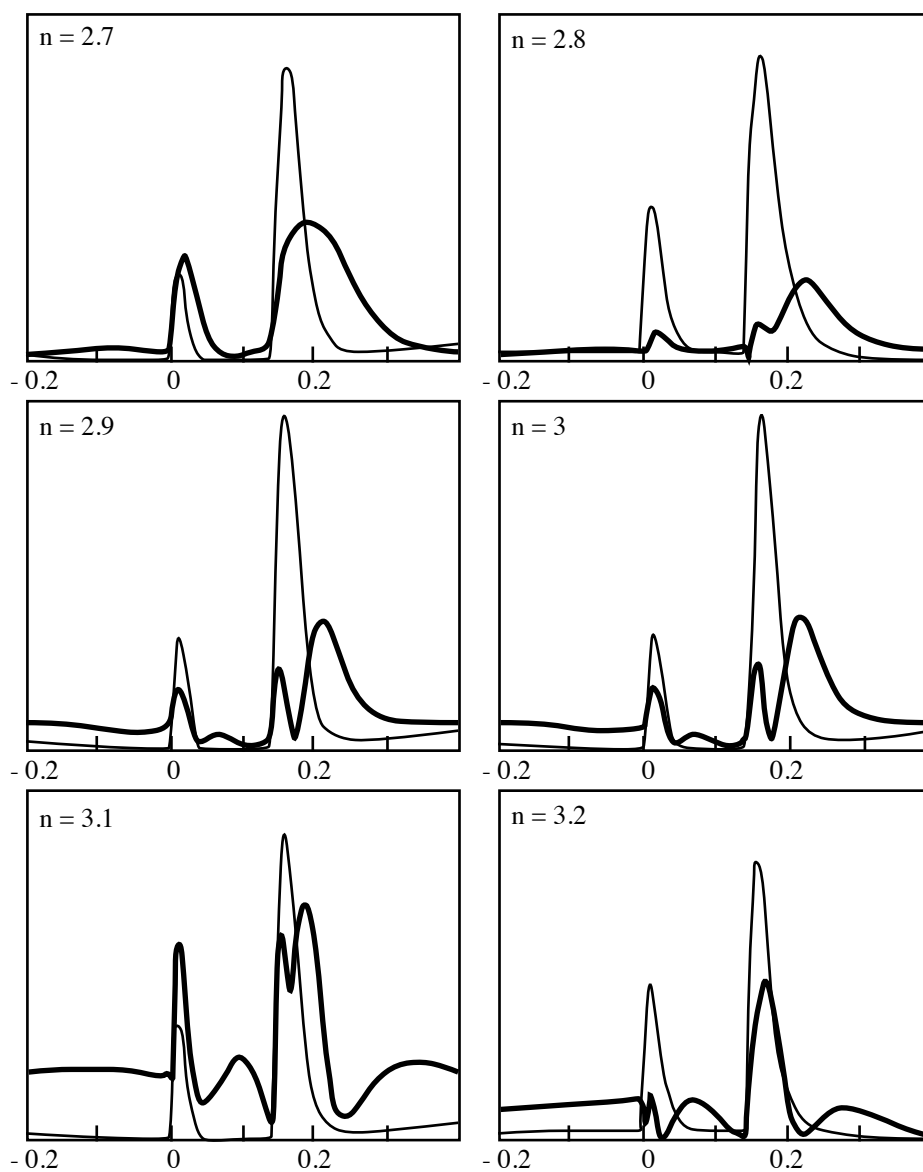


Figure 8. Simulated profiles of a pair of screw superpartials $1/2[110]$ in Co_3Ti . Fine lines correspond to two-beams simulations and thick lines correspond to simulations with four beams ($-g$, transmitted beam, $+g$ and $2g$) (x -axis in ξ_g unit). The images have been performed for the $g = 220$ beam while the ng beam is excited. The simulations have been calculated using a many-beams program without column approximation developed by C.J. Humphreys and modified in order to take into account of the anisotropy of the crystal (Oliver [8]).

3.3. DETERMINATION OF THE NATURE OF A STACKING FAULT IN Ni₃Al

Observations of dipoles of dislocations with a Burgers vector $1/3\langle 112 \rangle$ is a common feature in deformed Ni₃Al. These dipoles are faulted, and in order to determine the exact process of formation of these dipoles, it is of prime importance to know the fault vector of the defect.

Two cases are possible as a Superlattice Intrinsic Stacking Fault (SISF) or a Superlattice Extrinsic Stacking Fault (SESF) can be formed in the $\{111\}$ plane of the dipole. Simulations for different diffraction conditions (for different \mathbf{g}) are in accordance with observations of SISF rather than SESF (Figure 9).

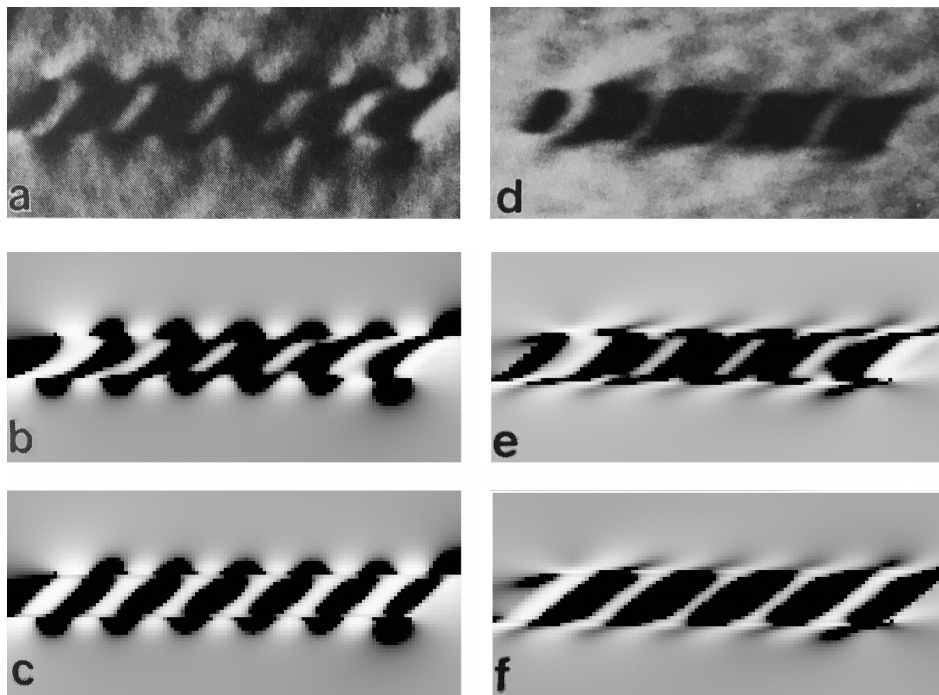


Figure 9 Comparisons of experimental and simulated images ; (a) Experimental dark field image with $\mathbf{g} = 1, 1, 1$ (b) simulated image with SISF ; (c) with SESF. (d) Experimental dark field image with $\mathbf{g} = 11, 1$, (e) simulated image with SISF ; (f) with SESF. The simulations have been performed using the program TWODIS, a two-beams program with column approximation (Head et al., [4]) (Experimental images, courtesy of P. Veyssière).

REFERENCES

1. Howie, A., and Whelan, M.J. (1961), *Proc. Roy. Soc.*, **A263**, 217.
2. Takagi, S (1962) *Acta Cryst.*, **15**, 1311.
3. Hirsch, P.B., Howie, A., Nicholson, R.B., Pashley, D.W., and Whelan, M.J., (1965) *Electron Microscopy of Thin Crystals*, Butterworths, London.
4. Head, A.K., Humble, P., Clarebrough, L.M., Morton, A.J., and Forwood, C.T. (1973) *Computed Electron Micrographs and Defects Identification*, North-Holland Publishing Company, Amsterdam.
5. Stroh, A.N. (1958) Dislocations and Cracks in Anisotropic Elasticity, *Phil. Mag.*, **3**, 625-646.
6. Steeds, J.W. (1973) *Introduction to Anisotropic Elasticity Theory of Dislocations*, Clarendon Press, Oxford.
7. Schäublin, R., and Stadelmann, P. (1993), A method for simulating electron microscope dislocation images, *Mater. Sci. and Eng. A*, **164**, 373-378.
8. Oliver, J. (1992) Structure fine des dislocations dans l'intermétallique Co_3Ti et simulation du contraste en faisceau faible, *PhD Thesis (in french)*, University of Paris XI - Orsay.